ORIGINAL ARTICLE

Real-Time In Vivo Characterization of Primary Liver Tumors With Diffuse Optical Spectroscopy During Percutaneous Needle Interventions

Feasibility Study in Woodchucks

Rami Nachabé, PhD, MSc, Benno H.W. Hendriks, PhD,† Ross Schierling, RT,‡ Jasmine Hales, VT,§ Judy M. Racadio, MD,‡ Sven Rottenberg, DVM,‖ Theo J.M. Ruers, MD, PhD,¶ Drazenko Babic, MD,* and John M. Racadio, MD‡*

Objective: This study presents the first in vivo real-time optical tissue characterization during image-guided percutaneous intervention using near-infrared diffuse optical spectroscopy sensing at the tip of a needle. The goal of this study was to indicate transition boundaries from healthy tissue to tumors, namely, hepatic carcinoma, based on the real-time feedback derived from the optical measurements.

Materials and Methods: Five woodchucks with hepatic carcinoma were used for this study. The woodchucks were imaged with contrast-enhanced cone beam computed tomography with a flat panel detector C-arm system to visualize the carcinoma in the liver. In each animal, 3 insertions were performed, starting from the skin surface toward the hepatic carcinoma under image guidance. In 2 woodchucks, each end point of the insertion was confirmed with pathologic examination of a biopsy sample. While advancing the needle in the animals under image guidance such as fluoroscopy overlaid with cone beam computed tomography slice and ultrasound, optical spectra were acquired at the distal end of the needles. Optical tissue characterization was determined by translating the acquired optical spectra into clinical parameters such as blood, water, lipid, and bile fractions; tissue oxygenation levels; and scattering amplitude related to tissue density. The Kruskal-Wallis test was used to study the difference in the derived clinical parameters from the measurements performed within the healthy tissue and the hepatic carcinoma. Kurtoses were calculated to assess the dispersion of these parameters within the healthy and carcinoma tissues.

Results: Blood and lipid volume fractions as well as tissue oxygenation and reduced scattering amplitude showed to be significantly different between the healthy part of the liver and the hepatic carcinoma ($P < 0.05$) being higher in normal liver tissue. A decrease in blood and lipid volume fractions and tissue oxygenation as well as an increase in scattering amplitude were observed when the tip of the needle crossed the margin from the healthy liver tissue to the carcinoma. The kurtosis for each derived clinical parameter was high in the hepatic tumor as compared with that in the healthy liver indicating intracarcinoma variability.

Conclusions: Tissue blood content, oxygenation level, lipid content, and tissue density all showed significant differences when the needle tip was guided from the healthy tissue to the carcinoma and can therefore be used to identify tissue boundaries during percutaneous image-guided interventions.

Key Words: near-infrared spectroscopy, hepatic carcinoma, interventional radiology, cone beam computed tomography

(*Invest Radiol* 2015;50: 443–448)

Received for publication January 5, 2015; and accepted for publication, after revision, January 29, 2015.

From the *Interventional X-ray Department, Philips Healthcare, Best; †In-Body Systems Department, Philips Research, Eindhoven, the Netherlands; Departments of ‡Radiology and §Veterinary Medicine, Cincinnati Children's Hospital Medical Center, Cincinnati, OH; and Departments of ‖Molecular Pathology and ¶Surgical Oncology, Netherland Cancer Institute, Amsterdam, the Netherlands.

Conflicts of interest and sources of funding: none declared.
Rami Nachabé, Benno H.W. Hendriks, and Drazenko Babic are employees of Philips.

Reprints: Rami Nachabé, PhD, MSc, Interventional X-ray Department, Philips Healthcare, Veenpluis 6, 5684 PC Best, the Netherlands.
E-mail: rami.nachabe@philips.com.

ISSN: 0020-9996/15/5007–0443

Last decade, the percentage of image-guided percutaneous biopsies has continuously increased at the expense of non–imaging-guided percutaneous approaches, which is likely related to the increasing use of advanced imaging modalities for biopsy guidance. As a consequence, recent trends indicate that radiologists will be performing an increasing amount of percutaneous needle biopsies. An increase of roughly 15% of biopsies by percutaneous approach over the last decade was observed across all anatomical regions.[1]

Nevertheless, despite the recent advances in imaging modalities to improve percutaneous needle guidance under imaging, biopsies do not always yield histological diagnostic samples. Diagnostic yield is dependent on several parameters such as lesion-related factors including lesion type and size as well as technical factors such as needle gauge, biopsied specimen size, amount of biopsied specimens within a lesion, and type of imaging modality for guidance. Most commonly used modalities are fluoroscopy, ultrasound (US), computed tomography (CT), CT fluoroscopy, magnetic resonance (MR) imaging, and, more recently, multimodality such as 3-dimensional (3D) fluoroscopy consisting of combining cone beam CT (CBCT) with live fluoroscopy from a C-arm system[2] or even either positron emission tomography, CT, or MR overlaid with 3D fluoroscopy.[3–6]

Diffuse optical spectroscopy (DOS) is an emerging technique for optical tissue characterization. This technique consists of studying the spectral light response after illuminating tissue with a light source. The collected optical spectra are translated into clinically relevant parameters such as blood, water, lipid, and bile fractions; tissue oxygenation levels; and tissue density related to the scattering of light.[7] In recent research, several advances have been made in integrating optical fibers into needlelike probes for DOS measurements at the distal end of the devices.[8–10] Most of the DOS clinical studies have addressed the diagnostic performance in discriminating tumors from the normal tissue. These clinical experiments consisted of performing several point measurements at different locations in tumors and healthy tissue. The diagnostic performance of DOS has generally been evaluated by comparing the tissue classification from the measurements with the actual tissue type as identified with pathologic examination[8,9] or diagnostic medical imaging.[8,10] A few in vivo studies have been conducted to demonstrate that DOS enables tissue discrimination, namely, discrimination of malignant tissue from healthy tissue.[8–10] In most of these cases, image guidance was used to confirm the location of the tip of the probe.[8,10] All of the studies investigated the diagnosis performance of DOS but not its ability to provide the physician with real-time feedback on the guidance of the needle from normal to tumor tissue based on DOS. We hypothesize that continuous measurements would be of great relevance during percutaneous procedures because they enable detection of the transition from healthy tissue to tumor based on the clinical parameters derived from optical spectroscopy. In

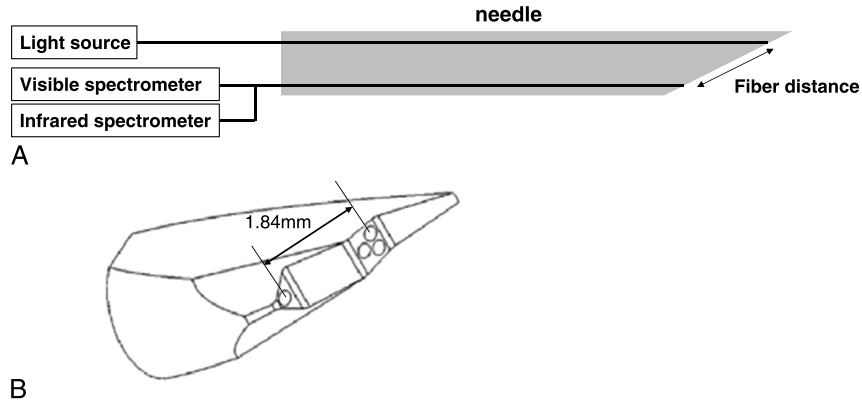

FIGURE 1. Schematic drawing of the optical setup (A) and the design of the optical needle tip (B).

addition, it would provide a profile of the tissue along the needle path yielding data on intrasubject heterogeneity.

To this aim, we applied continuous DOS measurements under 3D fluoroscopy and US guidance in woodchucks with hepatocellular carcinoma (HCC) tumor to evaluate the added value of continuous measurements during percutaneous insertions.

MATERIALS AND METHODS

Animal Model and Measurement Protocol

All procedures in this study followed the guidelines of the Institutional Animal Care and Use Committee of Cincinnati Children's Hospital Medical Centre and were approved by the ethics committee.

Five woodchucks with HCC induced by the woodchuck hepatitis virus infection were used; they were ordered from Northeastern Wildlife Inc and weighed an average of 2.5 kg. The animals were initially sedated with an intramuscular injection of 5 mg/kg of xylazine (Fort Dodge Laboratories, Kansas City, MO) and 50 mg/kg of ketamine (Fort Dodge Laboratories). All animals were placed under general anesthesia by using 1% to 5% isoflurane (Halocarbon Products Co, New Jersey, NY) administered through endotracheal tube. For intravenous contrast agent administration, a 20-gauge angiocatheter (Cook Medical Inc, Bloomington, IN) was placed into the femoral vein using direct US guidance after shaving the skin of the animals and making a small incision. Each animal was used for 2 to 4 separate needle insertions with associated measurements and was then euthanized at the end of the experimental day with an intravenous injection of 1 mL/5 kg of Fatal-Plus (Vortech Pharmaceuticals, Dearborn, MI).

Diffuse Optical Spectroscopy

A research prototype setup (Fig. 1A) that allows optical spectroscopy measurements of tissue via optical fibers integrated in a needle was used in this study.[7] In short, the setup includes a light source and 2 optical spectrometers that enable light detection in the visible and near-infrared wavelength range. A custom-made needle is connected to the light source and to both spectrometers via optical fibers. The optical needle is an 18-gauge needle with a 70-degree angled tip (Fig. 1B), whereas the fiber ends are cut straight. The fiber ends between source and detector fibers used in this study are 1.84 mm apart. This needle can perform optical spectroscopy measurements at its tip.

The light emitted at the tip of the needle travels through the tissue before reaching the collecting fiber and is subject to optical absorption and scattering. The measurement acquisition time per spectrum is 300 milliseconds. An analytical model was used to derive the various physiological and morphological properties from each spectrum using a mathematical model that describes tissue-light interaction.[7]

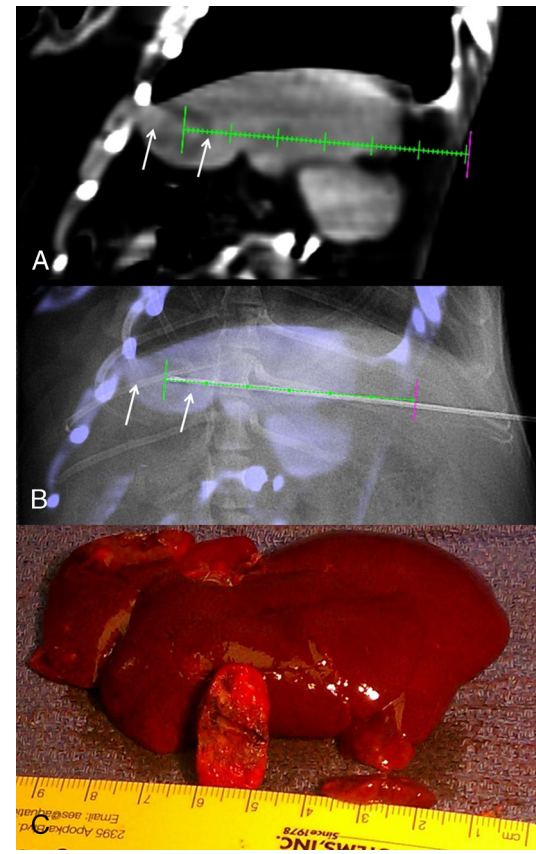

FIGURE 2. A, Cone beam CT slice depicts a virtual needle path (green line) with the entry point (magenta marker) defined at the skin surface and the end target in the middle of the round tumor. The small and large dash markers along the virtual line correspond to millimeter and centimeter spacing, respectively. The white arrows indicate the boundaries of the tumor along the virtual line (B). Cone beam CT overlayed with live fluoroscopy (ie, 3D fluoroscopy) demonstrates the tumor in the liver (boundaries indicated by white arrows). The green line corresponds to the virtual needle trajectory. The needle has been advanced along the virtual needle path, and the tip is now in the center of the tumor. C, Photograph of the liver with a cut section through the tumor. The thickness of the tumor is roughly 1 cm as can also be seen in B and C. Figure 2 can be viewed online in color at www.investigativeradiology.com.

The physiological and morphological properties that were derived from each spectrum included biological volume fractions (blood, water, lipid, and bile), oxygenation level of blood, and light scattering due to tissue density.

Image Guidance

The needle insertions were performed under 3D fluoroscopy (XperGuide; Philips Healthcare, Best, the Netherlands). Whereas US is a common imaging technique used for needle guidance, 3D fluoroscopy is a more recent technique that consists of overlaying live x-ray fluoroscopy with CBCT.[2] A 3D soft tissue CBCT data set was acquired after injection of a contrast agent (Optiray 350; Covidien, Hazelwood, MI) for better visualization of the tumor and the surrounding healthy tissue. From the 3D data set, an optimal CBCT slice with the tumor clearly visible was selected to define a planned needle path. The needle planning was interactively performed by drawing a line from the center of the tumor toward the skin surface (Fig. 2). Live 3D fluoroscopy and US imaging were acquired simultaneously with DOS acquisition to assure registration of the tissue characterization with the actual location of the needle tip. A total of 9 insertions were performed in the animals. At the end of the experiment, the liver was excised for gross tissue investigation. A cut-through was performed along the needle path in the tumor to observe the tissue structure, and a tissue biopsy at the last position of the needle was obtained for histological investigation.

Data Collection and Analysis

While the needle was advanced under live 3D fluoroscopy, optical spectra were acquired every 300 milliseconds and the real-time data analytical model converted the data into clinical information listed in the previous section concerning DOS. Once the final target was reached, a biopsy was taken for further pathologic investigation and correlation with the DOS information.

Pathologic Analysis

The obtained tissue samples after being fixated in formalin were paraffin-embedded, cut in approximately 2-μm-thick sections, and stained with hematoxylin and eosin staining. The slices were histologically investigated by a veterinary pathologist.

Statistical Analysis

For each of the parameters derived from the spectral measurements, statistical analyses were performed using the nonparametric Kruskal-Wallis test for differences between normal and tumor for each insertion with a significance level of 5%. Kurtoses were computed to assess the dispersion for each parameter derived from measurements in both types of tissue. All statistical analyses were done with a data processing software (MATLAB; MathWorks, Natick, MA).

RESULTS

In the liver of the woodchucks, typically more than 1 lesion was present. In Figure 3, an example of excised liver with tumors is shown, revealing at least 3 different types of lesions. For the locations indicated in Figure 3B, pathology was performed with the images of the slides shown in Figure 3, C to F, with corresponding measured optical spectra shown in Figure 3, G to J. The 3 lesions, cut open in Figure 3B, have a different macroscopic appearance, which is also reflected in observable differences in the spectra. The histology images of the different locations show that, in addition to the liver neoplasia, there is multifocal necrosis with neutrophils and macrophages as well as fibrosis, which indicates chronic hepatitis and cirrhosis. The tumors are of the trabecular type and solid type. The neoplasms lack portal areas but otherwise still resemble the liver architecture. Nuclear pleomorphism is limited, as well as the mitotic figure, indicating that these neoplasms are borderline carcinomas. In the necrotic lesion 4 of Figure 3F, a high amount of fat droplets is observed. The corresponding optical spectrum (Fig. 3J) reveals a

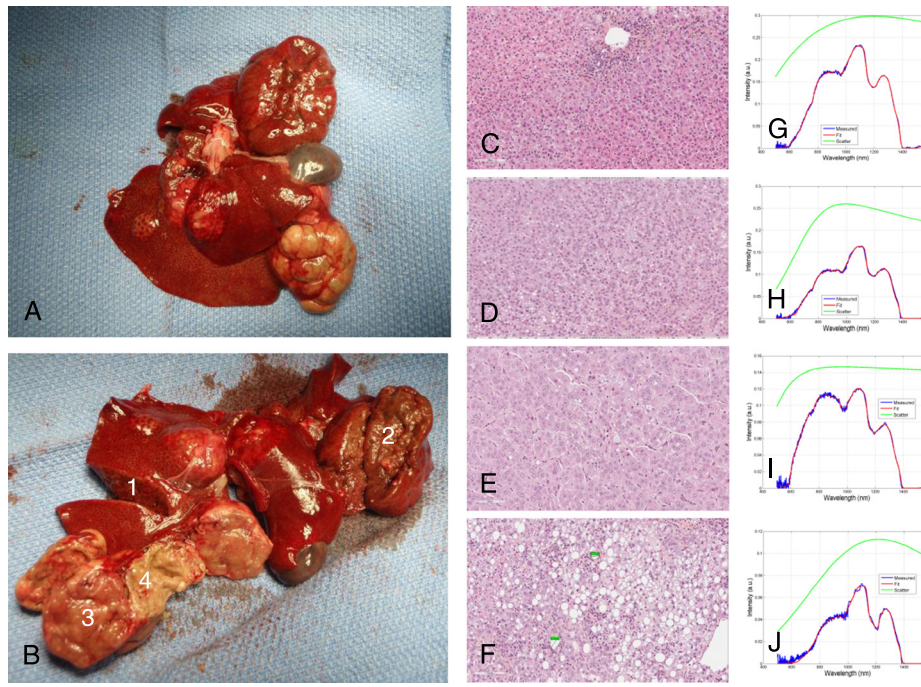

FIGURE 3. A and B, Pictures of an excised liver of one of the woodchucks. Tissue samples were taken at locations 1 to 4 with corresponding pathology shown in C to F and optical spectra shown in G to J, respectively. G–J, The blue line is the measured spectrum, the red line is the fitted spectrum, and the green line is the scattering contribution to the spectrum determined by fitting. Figure 3 can be viewed online in color at www.investigativeradiology.com.

TABLE 1. Mean (SD) for Each Derived Parameter and Each Insertion

	Normal	Tumor
Insertion 1	n = 38	n = 31
Blood volume fraction*	13.2 (4.4)	7.5 (5.6)
Tissue oxygenation*	19 (9)	3.3 (5.8)
Lipid volume fraction*	7 (2)	5 (3)
Scattering amplitude*	11.0 (1.2)	11.6 (1)
Bile volume fraction*	3 (2)	4 (1)
Collagen volume fraction*	2 (1)	9 (2)
Insertion 2	n = 50	n = 15
Blood volume fraction*	19.4 (2.6)	16.1 (0.8)
Tissue oxygenation*	85 (10)	69 (1)
Lipid volume fraction*	25 (9)	9 (2)
Scattering amplitude*	9.3 (0.5)	9 (0.1)
Bile volume fraction	0 (0)	0 (0)
Collagen volume fraction*	8 (7)	21 (3)
Insertion 3	n = 37	n = 120
Blood volume fraction*	9.1 (3.5)	6.3 (2.5)
Tissue oxygenation*	53 (16)	30 (15)
Lipid volume fraction*	6 (8)	11 (7)
Scattering amplitude*	9.4 (1.7)	11.5 (1.3)
Bile volume fraction	8 (2)	7 (1)
Collagen volume fraction*	22 (11)	5 (3)
Insertion 4	n = 10	n = 47
Blood volume fraction*	5.7 (0.6)	0.9 (0.7)
Tissue oxygenation*	55 (2)	22 (8)
Lipid volume fraction*	4 (1)	1 (1)
Scattering amplitude*	8.5 (0.2)	11.3 (1.8)
Bile volume fraction*	4 (1)	1 (1)
Collagen volume fraction*	0 (0)	3 (1)
Insertion 5	n = 44	n = 16
Blood volume fraction*	19.5 (1.9)	2.8 (2.4)
Tissue oxygenation*	65 (3)	35 (20)
Lipid volume fraction*	5 (1)	4 (1)
Scattering amplitude	6.3 (0.6)	7.4 (2.2)
Bile volume fraction*	7 (1)	1 (1)
Collagen volume fraction*	2 (2)	0 (0)
Insertion 6	n = 11	n = 69
Blood volume fraction	15.2 (4.3)	17.9 (4.3)
Tissue oxygenation*	75 (2)	72 (2)
Lipid volume fraction*	4 (1)	2 (1)
Scattering amplitude*	6.4 (0.3)	8.6 (0.8)
Bile volume fraction*	4 (1)	7 (1)
Collagen volume fraction*	0 (0)	0 (0)
Insertion 7	n = 65	n = 55
Blood volume fraction	6.2 (0.3)	6.7 (3.3)
Tissue oxygenation*	46 (5)	15 (11)
Lipid volume fraction*	45 (1)	16 (13)
Scattering amplitude	26 (1)	25 (14)
Bile volume fraction*	1 (1)	5 (3)
Collagen volume fraction	4 (3)	3 (5)
Insertion 8	n = 73	n = 64
Blood volume fraction*	52.7 (6.3)	12.6 (9.4)
Tissue oxygenation*	38 (18)	10 (11)
Lipid volume fraction*	15 (6)	25 (6)
Scattering amplitude*	12.7 (0.9)	19.7 (8.3)
Bile volume fraction	2 (2)	1 (2)
Collagen volume fraction*	1 (3)	7 (11)
Insertion 9	n = 231	n = 50
Blood volume fraction*	8.7 (4.1)	2.8 (3.1)
Tissue oxygenation*	72 (15)	32 (15)
Lipid volume fraction*	20 (25)	70 (28)
Scattering amplitude	13.7 (9.9)	14.1 (21.5)
Bile volume fraction	1 (1)	0 (0)
Collagen volume fraction*	4 (4)	1 (2)

Mean (SD) of the estimated blood volume fraction, blood oxygenation, lipid volume fraction, scattering amplitude, bile volume fraction, and collagen fraction in healthy and tumor tissues for 9 insertions.

*Statistical significant difference.

n indicates the amount of acquired spectra.

Continued next page

sharp absorption peak of approximately 1200-nm wavelength indicative of the presence of a significant amount of fat.

Blood and lipid volume fractions and tissue oxygenation were significantly greater in normal livers as opposed to tumors (Table 1), whereas the scattering amplitude was greater in the tumors than in normal liver tissue ($P < 0.05$). Within each insertion, the transition from healthy to tumor tissue is identified as a significant decrease in blood and lipid content and oxygenation level and as an increase in scattering amplitude (Figs. 4, 5). The observation that blood was more abundant in healthy liver tissue correlates with the macroscopic investigations after tissue resection (Figs. 2C, 3). The kurtosis values indicate that there is a higher dispersion of the obtained parameter values in tumor than in healthy tissue (Table 2). For instance, the scattering amplitude in healthy liver tissue is homogeneous, whereas it is heterogeneous in the tumor; this correlates with the gross observation that the tumor tissue has a more granular structure (Figs. 2C, 3). In addition, the difference in tissue homogeneity between the tumor and the healthy part of the liver is visible on the CBCT images (Fig. 2A). Bile content was not significantly different between normal and tumor tissues with

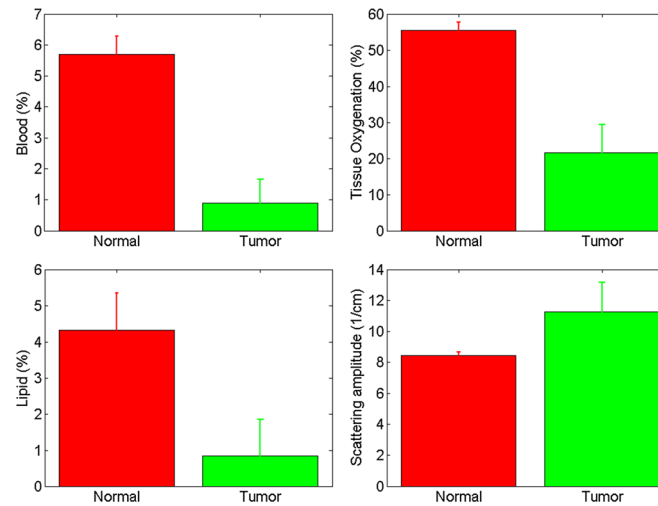

FIGURE 4. Bar plots with error bars indicating mean and standard deviation of blood and lipid volume fractions, tissue oxygenation, and scattering amplitude for a single insertion in healthy and tumor tissue within a single animal. Figure 4 can be viewed online in color at www.investigativeradiology.com.

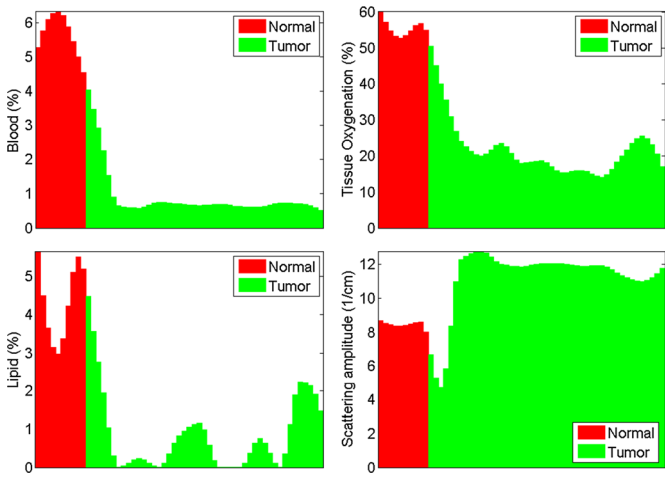

FIGURE 5. Histogram of blood volume fraction, tissue oxygenation, lipid volume fraction, and scattering amplitude derived from DOS measurements performed as the needle was inserted from normal to tumor tissue within a single animal. These data are the source from which the bar plots in Figure 2 were obtained. Figure 5 can be viewed online in color at www.investigativeradiology.com.

values of 2% ± 2% and 3% ± 3%, respectively ($P = 0.65$). Most of these findings were consistent for all 9 insertions except for 1 case in which the blood content, blood oxygenation, and fat content were comparable in the tumor tissue and normal tissue.

DISCUSSION

To our knowledge, there have been no previous in vivo liver tumor DOS studies, although there have been a few ex vivo studies that demonstrate higher scattering amplitude as well as higher lipid, blood, and bile content in the healthy liver compared with those in the tumor. However, care should be taken in interpreting ex vivo human studies because the tissue properties can change very quickly after excision of the tissue.[5] Moreover, the ex vivo studies were done in liver with colorectal metastases, whereas the present study addresses primary liver tumors; the comparison of the derived parameters is thus not straightforward. Therefore, this present in vivo animal study can be considered as a starting point for future investigations in discriminating HCC from healthy liver tissue with the DOS technique.

All the woodchucks had signs of chronic infections. This means that this study shows that the DOS technique can distinguish between nontumorous liver tissue (with moderate multifocal degeneration and fibrosis [cirrhosis]) and tumor tissue.[11,12]

In our study, there was no significant difference in the bile content, which is most likely due to the fact that the animals have primary tumors and not metastases from other organs; metastases are made of abnormal cells from the organ of origin; therefore, no bile is expected in metastases.[13]

The existing in vivo studies in the literature were mainly performed in the breast[8,9] and the lung[2]; therefore, only comparisons of physiological parameters (eg, oxygenation levels and scattering amplitude) in our study to these previous studies are valid, and tissue composition comparisons are not valid. Our results agree with the general reported findings from the in vivo human DOS studies.[8–10] These studies demonstrated lower oxygenation levels in the tumor and higher scattering amplitude, as did our study. However, our study evaluated the spectral and clinical variations along a needle path as opposed to a single-point measurement[8–10] yielding additional information with respect to the variation in tissue composition across the tumor as well as identifying the boundary between healthy and tumor tissue. To discriminate a tumor tissue from a nontumor tissue, a discrimination method

TABLE 2. Kurtosis of Each Derived Parameter and for Each Insertion

	Normal	Tumor
Insertion 1		
Blood volume fraction	2.9	2.0
Tissue oxygenation	1.4	11.4
Lipid volume fraction	1.3	2.9
Scattering amplitude	1.7	2.0
Bile volume fraction	1.5	2.2
Collagen volume fraction	2.7	4.6
Insertion 2		
Blood volume fraction	1.4	4.2
Tissue oxygenation	1.4	5.8
Lipid volume fraction	1.8	4.0
Scattering amplitude	1.8	2.1
Bile volume fraction	10.0	2.3
Collagen volume fraction	2.2	4.2
Insertion 3		
Blood volume fraction	2.3	3.0
Tissue oxygenation	3.8	2.5
Lipid volume fraction	2.8	1.7
Scattering amplitude	3.4	1.9
Bile volume fraction	1.6	3.5
Collagen volume fraction	2.0	3.0
Insertion 4		
Blood volume fraction	2.2	11.9
Tissue oxygenation	3.0	7.5
Lipid volume fraction	1.5	5.7
Scattering amplitude	4.0	8.1
Bile volume fraction	1.8	28.5
Collagen volume fraction	1.4	3.8
Insertion 5		
Blood volume fraction	10.2	4.0
Tissue oxygenation	2.0	1.8
Lipid volume fraction	4.3	4.8
Scattering amplitude	2.1	2.4
Bile volume fraction	3.7	7.4
Collagen volume fraction	1.5	6.7
Insertion 6		
Blood volume fraction	2.0	3.5
Tissue oxygenation	6.8	5.2
Lipid volume fraction	1.9	2.0
Scattering amplitude	1.5	4.5
Bile volume fraction	2.0	3.3
Collagen volume fraction	1.6	11.8
Insertion 7		
Blood volume fraction	1.9	2.7
Tissue oxygenation	2.3	1.7
Lipid volume fraction	2.5	2.1
Scattering amplitude	2.4	11.0
Bile volume fraction	2.0	1.7
Collagen volume fraction	2.8	6.1
Insertion 8		
Blood volume fraction	2.6	6.8
Tissue oxygenation	2.1	3.6
Lipid volume fraction	2.4	5.2

Continued next page

TABLE 2. *(Continued)*

	Normal	Tumor
Scattering amplitude	3.5	1.4
Bile volume fraction	3.6	2.3
Collagen volume fraction	27.2	5.4
Insertion 9		
Blood volume fraction	3.5	4.1
Tissue oxygenation	2.2	2.9
Lipid volume fraction	4.3	3.5
Scattering amplitude	11.0	10.4
Bile volume fraction	2.7	7.3
Collagen volume fraction	2.8	5.6

Kurtosis of the estimated blood volume fraction, blood oxygenation, lipid volume fraction, scattering amplitude, bile volume fraction, and collagen fraction in healthy and tumor tissues for 9 insertions.

based on multiple parameters is required to cope with tumor variability and heterogeneity. Our study suggests that blood content and oxygenation, lipid content, and scattering are the most promising parameters that should be further investigated on a larger data set. The information provided by DOS, such as mapping of blood oxygenation levels along the needle path, can be of great relevance in the case of biopsy procedures. Hypoxic tissue is often associated with necrosis; therefore, measuring the oxygenation level in tumors can allow the operator to avoid performing a biopsy in a necrotic region that would not allow conclusive tumor staging by pathologists. Hence, relying on the oxygenation level in blood is of great interest in performing biopsies.[9]

In the HCC tumors, the estimated lipid volume fraction and the pathology slides showed a nonuniform distribution, which is expected because HCC is known to be associated with patchy macroscopic fatty change.[14] The scattering amplitude related to tissue density is also heterogeneous in the tumor, whereas it is more homogenous in the healthy liver. This observation is in agreement with existing findings on stiffness measurements with US or MR elastography, with tumors being stiffer than normal liver tissue.[15]

Changes in the blood content, tissue oxygenation, and scattering were most notable near the tumor boundary, as can also be observed in Figure 5. This observation would enable taking biopsies near the tumor boundary where the likelihood of harvesting vital tissue is greater because necrosis typically starts in the center of the tumor.

In the last couple of years, a focus on image-based analysis were developed and validated for HCC diagnosis and staging using CT perfusion and optical-based tomography such as bioluminescence.[16–18] These new developments enable more accurate identification of the accurate location to be treated that can be used for road map navigation for interventional radiologists or surgeons for treatment or resection. The drawback of 3D fluoroscopy is that the information is more qualitative than quantitative although it benefits of real-time imaging for device navigation. More recently, similarly to the presented needle with DOS sensing as it tips, Kang et al[19] developed an electrode with electromagnetic tracking in US radiofrequency ablation for an improved positioning of the probe to radiate, in an effective way, most of the tumor to avoid recurrence.[19]

In conclusion, this study shows the potential of real-time tissue characterization by DOS measurements at the tip of a needle image-guided intervention. This first in vivo liver study using diagnostic imaging as a reference demonstrates that blood content and tissue oxygenation can be used as the primary discriminators for transition from normal tissue to tumor. Lipid content and scattering amplitude provide information on the heterogeneity of tissues along the needle path. Ultimately, this technology allowing real-time tissue composition feedback during percutaneous intervention would provide diagnostic information on the nature of the tumor to immediately treat it (eg, ablation, embolization) without needing to perform a biopsy for pathologic evaluation of the tumor and have the patient to come back for a therapeutic intervention.

ACKNOWLEDGMENTS

The authors thank Jarich Spliethoff for the tissue handling in the pathology department.

REFERENCES

1. Kwan SW, Bhargavan M, Kerlan RK, et al. Effect of advanced imaging technology on how biopsies are done and who does them. *Radiology*. 2010;256:751–758.
2. Spelle L, Ruijters D, Babic D, et al. First clinical experience in applying XperGuide in embolization of jugular paragangliomas by direct intratumoral puncture. *Int J Comput Assist Radiol Surg*. 2009;4:527–533.
3. Racadio JM, Babic D, Homan R, et al. Live 3D guidance in the interventional radiology suite. *Am J Roentgenol*. 2007;189:W357–W364.
4. Cooke DL, Levitt M, Kim LJ, et al. Intraorbital access using fluoroscopic flat panel detector CT navigation and three-dimensional MRI overlay. *J Neurointerv Surg*. 2010;2:249–251.
5. Abi-Jaoudeh N, Mielekamp P, Noordhoek N, et al. Cone-beam computed tomography fusion and navigation for real-time positron emission tomography-guided biopsies and ablations: a feasibility study. *J Vasc Interv Radiol*. 2012;23:737–743.
6. Floridi C, Radaelli A, Abi Jaoudeh N, et al. C-arm cone-beam computed tomography in interventional oncology: technical aspects and clinical applications. *Radiol Med*. 2014;119:521–532.
7. Nachabe R, Hendriks BHW, van der Voort M, et al. Estimation of biological chromophores using diffuse optical spectroscopy: benefit of extending the UV-VIS wavelength range to include 1000 to 1600 nm. *Biomed Opt Exp*. 2010;1:1432–1442.
8. Brown JQ, Vishwanath K, Palmer GM, et al. Advances in quantitative UV-visible spectroscopy for clinical and pre-clinical application in cancer. *Curr Opin Biotechnol*. 2009;20:119–131.
9. Van Veen RL, Amelink A, Menke-Pluymers M, et al. Optical biopsy of breast tissue using differential path-length spectroscopy. *Phys Med Biol*. 2005;50:2573–2581.
10. Kanick SC, van der Leest C, Djamin RS, et al. Characterization of mediastinal lymph node physiology in vivo by optical spectroscopy during endoscopic ultrasound-guided fine needle aspiration. *J Thorac Oncol*. 2010;5:981–987.
11. Tennant BC, Gerin GL. The woodchuck model of hepatitis B virus infection. *ILAR J*. 2001;42:89–102.
12. Jeong DH, Jeong WI, Chung JY, et al. Hepatic cirrhosis in a young woodchuck (*Marmota monax*) due to vertical transmission of woodchuck hepatitis virus (WHV). *J Vet Sci*. 2003;4:199–201.
13. Nachabe R, Evers DJ, Hendriks BHW, et al. Effect of bile absorption coefficients on the estimation of liver tissue optical properties and related implications in discriminating healthy and tumorous samples. *Biomed Opt Exp*. 2011;2:600–614.
14. Prasad SR, Wang H, Rosas H, et al. Fat-containing lesions of the liver: radiologic-pathologic correlation. *Radiographics*. 2005;25:321–331.
15. Mariappan YK, Glaser KJ, Ehman RL. Magnetic resonance elastography: a review. *Clin Anat*. 2010;23:497–511.
16. Jiang T, Kambadakone A, Kulkami NM, et al. Monitoring response to antiangiogenic treatment and predicting outcomes in advanced hepatocellular carcinoma using image biomarkers, CT perfusion, tumor density, and tumor size (RECIST). *Invest Radiol*. 2012;47:11–17.
17. Thompson SM, Callstrom MR, Knudsen BE, et al. Molecular bioluminescence imaging as a noninvasive tool for monitoring tumor growth and therapeutic response to MRI-guided laser ablation in a rat model of hepatocellular carcinoma. *Invest Radiol*. 2013;48:413–421.
18. Wu D, Tan M, Zhou M, et al. Liver computed tomographic perfusion in the assessment of microvascular invasion in patients with small hepatocellular carcinoma. *Invest Radiol*. 2015;50:188–194.
19. Kang TW, Lee MW, Choi SH, et al. A novel electrode with electromagnetic tip tracking in ultrasonography-guided radiofrequency ablation: a phantom ex vivo, and in vivo experimental study. *Invest Radiol*. 2012;47:11–17.